Packaging of Dual-Mode Wireless Communication Module Using RF/Optoelectronic Devices With Shared Functional Components

Jun Liao, *Member, IEEE*, Juan Zeng, *Member, IEEE*, Shengling Deng, *Member, IEEE*, Anatoliy O. Boryssenko, Valencia M. Joyner, *Member, IEEE*, and Zhaoran Rena Huang, *Member, IEEE*

***Abstract*—This paper reports the design, fabrication, and testing of a compact radio-frequency (RF)/ free space optical (FSO) dual mode wireless communication system. A modified split dual-director quasi-Yagi antenna is integrated with optical transmitter and receiver by sharing layout structural components. Bare die vertical-cavity surface-emitting laser (VCSEL) and P-i-N photodiode (PIN) are placed on antenna director pads and wire bonded to printed circuit board (PCB)-mounted laser driver and transimpedance amplifier (TIA) circuits. Detailed analysis of coupling between RF channel and associated electrical connections for the FSO channel is presented using commercial simulation tools to predict its impact on link degradation. Although crosstalk appears between RF and optical channels, the prototyped system demonstrated dual-mode high-rate communication capability with measured 2.5 Gb/s data rate in FSO link. Variations in RF subsystem features due to coupling from the FSO subsystem is estimated through radiation pattern measurement using near-field scanner.**

***Index Terms*—Dual mode communication, free space optics, hybrid packaging, quasi-Yagi antenna, signal integrity.**

I. Introduction

HYBRID wireless communication systems, combining free space optical (FSO) and radio-frequency (RF) transmission, will play a key role in providing future-generation networks with increased data capacity, agility, and reduced power consumption, size, and cost. In the past few years, extensive work has been done to exploit the network connectivity, routing, and coding of communication channels [1]–[5] for hybrid RF-FSO networks. However, the hardware development of a fully integrated communication module that supports dual RF and FSO communication channels is still at its infancy. This paper presents the first attempt, to our knowledge, within the realm of packaging research to explore shared functional on-PCB components by both optical and RF elements.

Assembly of discrete components, monolithic integration, and hybrid packaging are the major packaging approaches at present. The assembly approach involves placement of the optical components and circuits in front of the RF antenna. The RF and free space optics share the same lens system for beam focusing [6]. Since the wavelength of the electromagnetic (EM) carrier for RF channel is much larger than the dimension of the optical elements, the blocking by the optical elements to the EM wave for the RF channel is negligible. The drawback of this approach is that the RF/optical (RF/opto) module is bulky in size, and typically not suitable for planar antenna system. There are a few variations of this packaging scheme. For example, the optical component and the RF antenna can also be placed at different locations on a printed circuit board (PCB) without a shared lens system [7]. In recent years, monolithic integration using a CMOS-compatible process has become an attractive alternative packaging approach to realize RF functions on the same chip with FSO devices [8]–[12]. Single-chip radio solutions featuring on-chip integrated zigzag dipole and resonant cavity antennas have been demonstrated [13]. However, there are two fundamental technical challenges intrinsic to this approach. First, large surface real estate is required for integrated on-chip antennas because the dimension of an antenna is on the same order as its free-space radiated wavelength, i.e., from a few centimeters at X-band to several millimeters at Ka-band and so on. Second, the antenna radiation efficiency is low due to the high loss tangent of the silicon substrate material as well as excitation of dissipative substrate modes.

Hybrid packaging is an alternative packaging scheme which utilizes a low loss tangent insulating substrate for the fabrication of antenna structures while the remaining circuit and optical elements are fabricated on a semiconductor substrate. In this paper, a new hybrid packaging approach is explored where the optical elements and RF microstrip antenna share common metal pads. A modified quasi-Yagi antenna with split director on Duroid board is adopted as the baseline antenna structure. The optical elements, namely photodetectors and laser diodes, are bonded to the antenna director pads. Hence, the metal pads play

Manuscript received January 17, 2009; revised October 24, 2009; accepted November 23, 2009. This research was supported in part by the Rensselaer Polytechnic Institute Internal Seed Grant, in part by Nation Science Foundation (NSF) under Award 0824068, in part by the NSF Smart Lighting Engineering Research Center (EEC-0812056), in part by Tufts University FRAC Award and the Center for Advanced Sensor and Communication Antennas, University of Massachusetts, Amherst under Air Force contract FA8718-06-C-0047. First published February 17, 2010; current version published May 05, 2010. This work was recommended for publication by Associate Editor R. Boudreau upon evaluation of the reviewers comments.

J. Liao, S. Deng, and Z. R. Huang are with the Department of Electrical, Computer, and Systems Engineering, Rensselaer Polytechnic Institute, Troy, NY 12180 USA (e-mail: liaoj2@rpi.edu; dengs@rpi.edu; zrhuang@ecse.rpi.edu).

J. Zeng and V. M. Joyner are with Department of Electrical and Computer Engineering, Tufts University, Medford, MA 02155 USA, (e-mail:juan.zeng@tufts.edu; vjoyner@ece.tufts.edu).

A. O. Boryssenko is with Department of Electrical and Computer Engineering, University of Massachusetts, Amherst, MA 01003 USA, (e-mail:boryssen@ecs.umass.edu)

Color versions of one or more of the figures in this paper are available online at http://ieeexplore.ieee.org.

Digital Object Identifier 10.1109/TADVP.2009.2038359

dual-roles in this packaging approach: supplying dc power and high-speed data signals to the optical devices, and directing the radiation of the EM wave for the RF communication channel. This novel approach gives rise to a new concept in packaging research towards miniaturization of electronic systems. One challenge of the RF/opto module using the new packaging approach in this paper is EM coupling between the metal structures associated with RF components and the optical elements. This effect and its system impact are explored in detail in this paper.

The proposed packaging scheme is used to prototype a compact hybrid RF/opto dual mode transceiver on Duroid (RT 6010) substrate commonly used for RF PCB designs. The RF/opto transceiver module is designed to achieve simultaneous operation of both RF and FSO communications with minimum interference between data transmitted on the RF and FSO channels. A data rate of up to 2.5 Gb/s for the FSO channel is demonstrated by the RF/opto module. This paper is organized as follows. Section II reports the fabrication and assembly of the RF/opto module. Section III presents and analyzes the performance of the RF channel of the RF/opto module. Section IV analyzes the signal degradation of the optical channel due to RF power coupling caused by sharing structural components. Section V reports the demonstration of an end-to-end dual-channel wireless RF and FSO links established between two packaged RF/opto modules.

II. RF/FSO Dual Mode Transceiver Packaging

A. Design of Split Dual-Director Quasi-Yagi Antenna

For the convenience of optical device integration, an antenna fabricated on a high permittivity substrate is preferred for the RF/opto transceiver module. A quasi-Yagi antenna was chosen for this work. The original quasi-Yagi antenna, shown in Fig. 1(a), is a broadband, high front-to-end ratio antenna that has maximum gain in the forward direction along the substrate plane [14]. The quasi-Yagi antenna consists of a transmission line feed, a balun, a coplanar strip line, a dipole drive, a director, and a ground plane reflector at the backside of Duroid substrate. The RF signal is fed through the SMA connector at the end of the antenna board. A power splitter follows the transmission line and divides the RF power into two parts to form a balun, which converts the unbalanced (common mode) microwave signal from transmission line into balanced (differential mode) feed mode. The RF signal passing through the coplanar strip line arrives at the dipole delta-gap feed point and radiates through the current-fed half-wave dipole. To get high radiation efficiency, the half-wave dipole should be fed with a balanced line to match the 73 Ω impedance of the antenna obtained theoretically. If a balanced antenna is fed with an unbalanced feeder, the common mode currents can cause the coplanar strip line to radiate in addition to the dipole element; thus the radiation pattern will be distorted. For the quasi-Yagi antenna of this work, as the transmission line carries unbalanced signal from the signal generator, the coplanar strip line and the dipole will receive unbalanced current if no balun is presented. Therefore, the balun is designed to introduce a 180° phase shift between the two arms of coplanar strip line. Balanced current signal is created and fed into dipole radiation element. The balun also provides an impedance match between the transmission line and coplanar strip line. The width of the balun line is optimized by full wave simulation. The director serves as the second passive radiation element. In order to package both photodetectors and optical emitters (i.e., laser diodes or light emitting diodes) on the antenna director pads, in this research, a modified quasi-Yagi antenna with splitting directors is explored. As shown in Fig. 1(b), the new design of the quasi-Yagi antenna has two rows of split-directors, which are served for dual functions: metal pads for the attachment and wire bonding of the photodetectors and laser diodes, and resonant structures for EM wave radiation of the RF channel. The photodetectors and laser diodes are attached to the split-directors. The detailed analysis of the split-director antenna will be discussed in the next section.

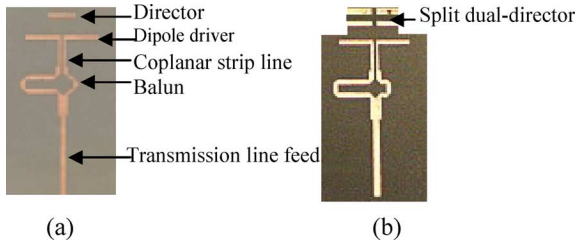

Fig. 1. (a) Photo of conventional quasi-Yagi antenna with partial ground conductor at the bottom. (b) Modified split dual-director quasi-Yagi antenna with partial ground conductor at the bottom.

Other novelty introduced in the design is alteration of the antenna direction of maximum radiation which is normally pointed along the antenna axis from the feed towards the aperture. In this design, the antenna provides unilateral radiation normal to its board surface because the antenna board is stacked above the major system PCB with the bottom ground conductor that alters the antenna beam. This allows integrating the RF and FSO front-ends and aligning the directions of optical and microwaving radiation. However, certain degradation of the antenna electrical features takes place [19] that is acceptable for the purpose of this study as further shown.

The split dual-director quasi-Yagi antenna is fabricated on a Duroid (RT 6010) board, which is constituted primarily of Polytetrafluoroethylene (PTFE) ceramic covered with rolled copper of 17 μm thickness. The Duroid substrate has a high dielectric constant ($\varepsilon_r = 10.2$) and low loss tangent (0.0023 at 10 GHz). The thickness of the Duroid board is 0.635 mm. We first patterned the front side of the quasi-Yagi antenna using photolithography process. Kapton tape is used as an etching protection mask to cover the back side of the Duroid board corresponding to the ground plane. Next, the copper on the Duroid board is etched using Ferric Chloride PCB etchant. Finally, an end-launch SMA connector is soldered to the antenna transmission line feed. More details about the fabrication have been reported in an earlier publication [15].

B. Assembly of Optical Components Onto Antenna Board

For the FSO link, a vertical-cavity surface-emitting laser (VCSEL) and a P-i-N photodiode (PIN) pairs are chosen to construct the end-to-end FSO transmitter and receiver due to their potential to expand to large arrays. In our design, we use a

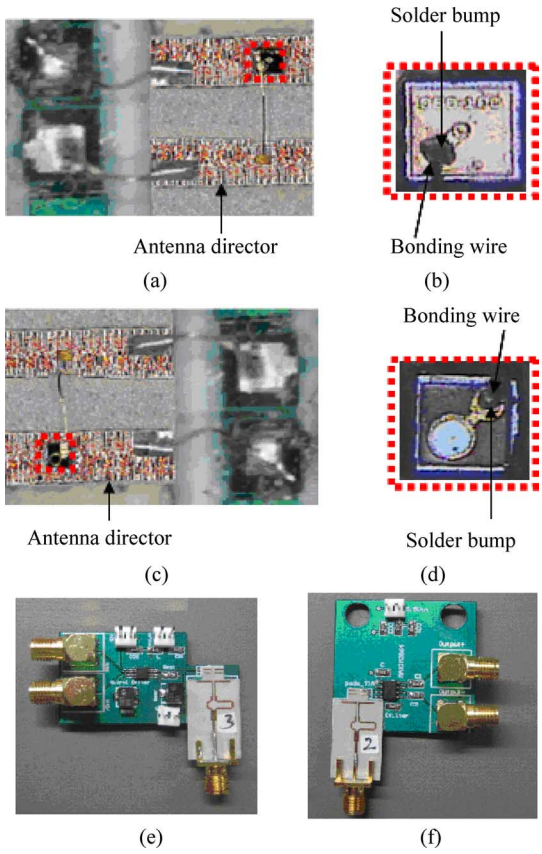

Fig. 2. Photo of the RF/FSO transceivers: (a) Packaging of VCSEL to transmitter board. (b) Bonding wire on VCSEL. (c) Packaging of PIN to transmitter board. (d) Bonding wire on PIN. (e) RF/opto transmitter board and (f) RF/opto receiver board.

bare die GaAs VCSEL (Optowell SM85-2N001) with emission at $\lambda = 850$ nm, and a PIN (Optowell SP85-3N001) to establish a high data rate optical link. Both VCSEL and PIN are 200 μm in height and have p-contact on the top surface and N contact at the bottom of the die. The die size is 300×300 μm^2 for the VCSEL and 250×250 μm^2 for the PIN, respectively. The VCSEL and PIN are attached to the antenna director pads by conductive epoxy adhesive (Resinlab SEC 1233). The epoxy is silver filled with two component curing, providing exceptionally high conductivity (0.0003 Ω-cm). The two components, base resin and catalyst, are mixed with 1:1 ratio in room temperature. A small droplet, $\sim$ 200 μm in diameter, is placed on the antenna director pad for the attachment of optical elements. First the VCSEL and PIN are placed on the epoxy drop, and then are cured in an oven at 60 °C for 1 h. The VCSEL is placed at the upper-left director and its p-contact is connected to the lower-left director by 1-mil gold wire bonding, shown in Fig. 2(a) and (b). PIN is placed at lower-left director and its p-contact is wire bonded to the upper-right director in Fig. 2(c) and (d).

C. Integrated RF/FSO Module

The antenna on Duroid board with the assembled laser diode and the photodetector is attached to a multi-layer FR4 PCB using epoxy adhesive (Loctite Hysol 608), on which the laser driver and transimpedance circuits are assembled. We prepared two packaged Duroid/PCB boards. One is the antenna board attached with laser diode and mounted on a PCB containing laser driver circuits, referred to as RF/opto transmitter board thereafter and shown in Fig. 2(e). The other one is the antenna board with photodetector packaged on the PCB with the transimpedance amplifier circuits, which is referred to as RF/opto receiver board thereafter and shown in Fig. 2(f). It is noted that the antenna is a RF component which can be used to broadcast EM wave and receive EM wave for the RF communication channel using standard RF measurement devices connected to the SMA antenna ports. The RF transceiver design itself is not included in this study.

Silver coated copper wires (UBA 3219) are used to electrically connect the antenna director pads to the optical circuit components as pictured in Fig. 2(a) and (b). The diameter of the wire is 0.25 mm and linear resistance is 0.5 Ω/m. The lateral distance from antenna director pads to the PCB bonding pads is 1 mm. As there is 0.635 mm height difference introduced by the Duroid board, the total wire length is estimated to be 1.2 mm. The inductance of the wire-pair is calculated using a twin lead transmission line model [16]

$$L_{\text{wire-pair}} \approx \frac{\mu_0 \mu_r}{\pi} \cosh^{-1} \frac{d}{2a} \tag{1}$$

where d is the distance between the two wires, a is the wire radius, μ_0 is the absolute permeability and μ_r is the relative permeability. For our case where $d = 1$ mm, $a = 0.125$ mm and $\mu_r = 1$, the calculated inductance is 1 nH. This inductance defined by (1) and capacitances associated with electrical leads and metal pads are shown to cause the degradation of optical signal integrity, which will be analyzed in detail in Section V.

On the RF/opto transmitter board, the high-speed current switch laser diode driver (Micrel SY88922V) is used to drive the laser diode. Utilizing the high-performance bipolar technology, the laser diode driver can operate up to 2.5 Gb/s with only 74 ps rise time and fall time. The modulation current is controlled by the bias current through the external resistor with a capability of driving a peak current of 30 mA. By tuning the external resistor for the modulation control, the output modulation current is varied linearly, which enables the best performance of the laser diode. With the supply voltage of 3.3 V, the differential output of the laser diode driver is modulated by the differential input pseudo-random bit sequence (PRBS) data with the desired current amplitude. The photograph of a packaged RF/FSO transmitter is shown in Fig. 2(e).

On the RF/opto receiver board, a transimpedance amplifier (TIA) MAX3864 is mounted to amplify the single-end photocurrent signal from the photodetector to a differential output voltage for measurement. With a single 3.0 V supply voltage and 0.85 pF source capacitance, the TIA achieves 2.0 GHz bandwidth, dynamic range of -24 dBm to 0 dBm and input-referred RMS noise as low as 490 nA. Therefore, it provides good performance when operating at bit rates up to 2.5 Gb/s. The photograph of the packaged RF/opto receiver is shown in Fig. 2(f).

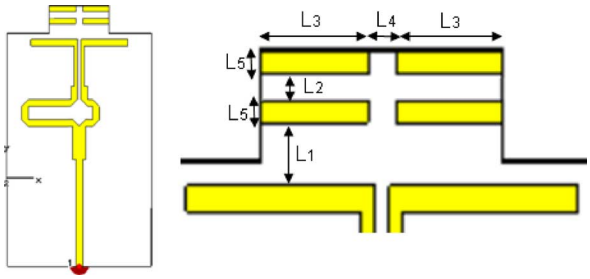

Fig. 3. CST model of split dual-director quasi-Yagi antenna.

III. RF Wireless Channel Design, Measurement, and Analysis

A. Modified Split Dual-Director Quasi-Yagi Antenna

The modified split dual-director quasi-Yagi antenna, which evolves from the log period dipole antenna (LPDA), is developed to meet the multi-functional requirements of our system. LPDA is inherently a broadband, multi-element, unidirectional antenna that can retain its electrical characteristics relatively constant over a wide range. For the antenna used in a hybrid RF/FSO system, it should not only exhibit broadband high gain radiation characteristics but also have a structure that is suitable for optical element assembly. Normally, LPDA consists of several dipole elements which are of different lengths and spacing to provide a 180° phase shift between alternating elements. However, for the convenience of optical element assembly, the directors in the modified antenna presented in this work have the same length and only the antenna driver is fed with differential signals. As the dipole driver radiates, the current will be induced in split dual-director. The conductor-split structure might support additional resonance and therefore broaden the overall bandwidth. These resonances are determined to the director dimensions, spacing between directors, and the nearby optical circuits. As we will discuss later in Sections IV and V, when optical device is assembled on one of the directors, and wire bonded to the other director, there is a current flowing through the bonding wires. This antenna induced current presents as a noise source to the optical signal. The amplitude of the current noise is studied using full wave simulation and verified by experimental measurement.

CST microwave studio is used to optimize the dimensions of the split dual-director pads. The simulation model used for the RF/FSO packaging is shown in Fig. 3. In the designed antenna version, the primary microstrip transmission line has an impedance of 50 Ω to be used with a standard SMA connector. This impedance is provided due to microstrip conductor dimensions of 0.6 mm in width and other parameters of the selected Duroid substrate discussed above. The split dual director and ground plane reflector at the bottom are designed to guide the antenna radiation. The modified antenna possesses the favorable property of the original one, such as high gain and broad bandwidth, but the radiation perpendicular to the antenna board plane is enhanced. This is done to match alignment of RF and FSO channels since vertical emitting laser diodes are used for the FSO channels.

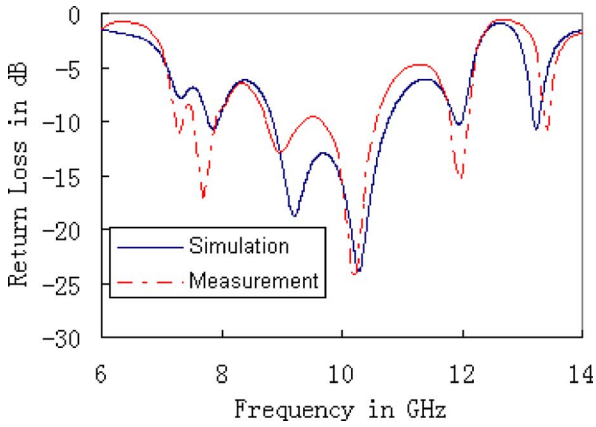

Fig. 4. Return loss of modified split dual-director quasi-Yagi antenna.

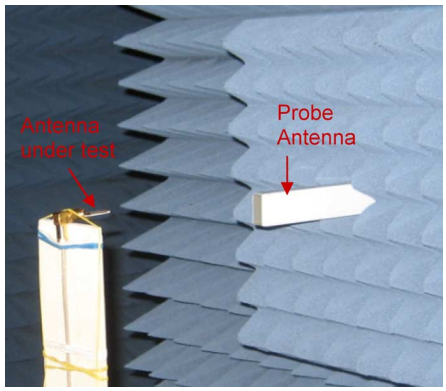

Fig. 5. Radiation pattern test setup in anechoic chamber.

By adjusting the parameters $L_1 \sim L_5$, the return loss is minimized in a wide band around 10 GHz with moderate broadband gain. The final design parameters (Fig. 3) are $L_1 = 1.7$ mm, $L_2 = 0.5$ mm, $L_3 = 2.4$ mm, $L_4 = 0.6$ mm, and $L_5 = 0.5$ mm. The remaining parameters for the antenna balun and primary dipole radiator are the same as reported in [14].

The modified split dual-director is fabricated according to the process described in Section II. Both the return loss and radiation pattern are measured before the assembly of the optical components.

Return loss of the antenna is measured by a network analyzer (Agilent 8510 C). As shown in Fig. 4, the modified antenna demonstrates low return loss at 10 GHz and has wide bandwidth in the X band. In addition, a good agreement between measured and predicted return loss is demonstrated in Fig. 4 to validate the employed design approach.

The radiation pattern of the antenna is measured by using a planar near-field scanner from Near Field System, Inc. (NSI) to sample the complex EM field which will be later converted to the far-field antenna radiation using the Fourier transform technique. The test setup is shown in Fig. 5. The split dual-director antenna under test is mounted on the top of the vertical arm of a wooden fixture. An open-waveguide probe antenna is placed 6 in apart in front of the test antenna aperture. The open-waveguide probe scans mechanically in a 22 in × 22 in area with a 0.5 in sampling step to record the amplitude and phase information of the EM fields at each sampling point. The open-waveguide

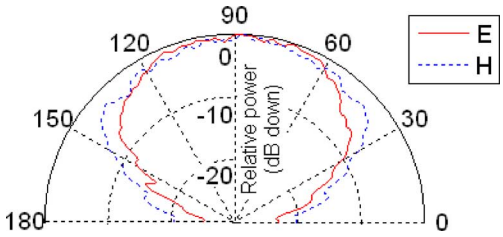

Fig. 6. Far field radiation pattern of modified quasi-Yagi antenna.

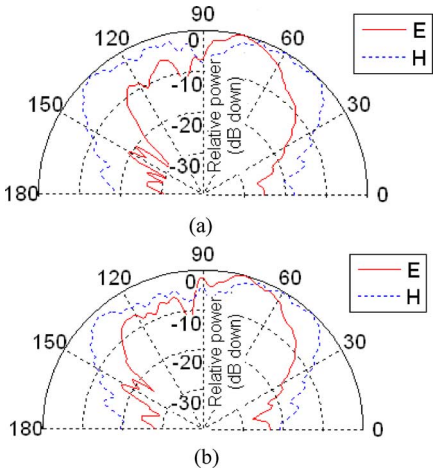

Fig. 7. Far field radiation pattern when VCSEL is (a) on and (b) off.

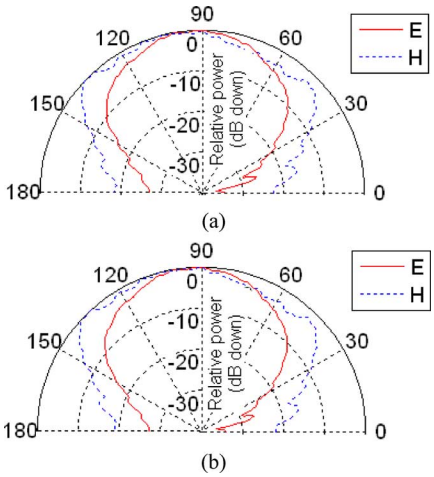

Fig. 8. Far field pattern of antenna on receiver board when PIN is (a) on and (b) off.

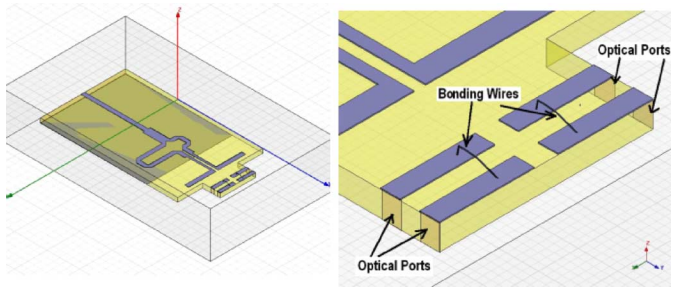

Fig. 9. Ansoft HFSS simulation model of the split dual-director quasi-Yagi antenna to predict coupling between the antenna driving port and four assigned optical ports. The coupling is modeled by the 5 × 5 complex scattering matrix.

probes measure co-polarization first and then rotates to 90° to measure cross-polarization at each sampling point. The whole scan area and both measured orthogonal field components followed by a probe compensation procedure enable deriving the antenna far-field pattern in a wide spatial cone [17], [18].

Having the measured near-filed and using the Fourier transform enable computation of the E- and H-plane sections of the far-field radiation patterns as plotted in Fig. 6. For the modified split dual-director quasi-Yagi antenna, the measured electric field amplitude of the co-polarized principal component is at least 10 dB larger than that of cross-polarized field component. This level of polarization purity is sufficient for the purposes of this study.

B. Testing Antenna on Transmitter Board

To evaluate how the coupling between RF and optical circuits that share the same on-PCB space and components affect antenna performance, we measure the radiation pattern of the antenna on the RF/FSO transmitter board. There is no noticeable change in radiation pattern when optical transmitter is on or off (Fig. 7). However, it is observed that the E-plane far field pattern of the antenna on the transmitter board degrades considerably (Fig. 7) compared with a single antenna without the optical transmitter (Fig. 6). The degradation is mainly due to the difference in electromagnetic environment for the single antenna and the same antenna integrated to the transmitter board [Fig. 2(c)]. In particular, there are several wiring terminals in close proximity to the antenna radiating structure that have connected wires laying parallel to the antenna principal E-plane polarization. As a result, the antenna electrical field becomes distorted being coupled to the nearby wires and so on. This unwanted effect will be tolerated in future studies by employing better on-board layout to minimize the pattern distortions.

C. Testing of Antenna on Receiver Board

For the antenna on the receiver board, the degradation in radiation pattern, as shown in Fig. 8, is not as prominent as that on the transmitter board. The antenna electromagnetic environment of this board is less affected by the nearby components of the optical circuits compared to the transmitter board. Also, there is no noticeable change of radiation pattern when PIN is turned on or off.

IV. Simulation of Coupling From RF to Optical Link

As the optical front-end transceivers are placed in the vicinity of the antenna printed conductors and share common structural components with the antenna, there is a leakage of RF energy into FSO link and vice versa. This phenomenon might lead to operational complications and needs to be explored in details. For this, we use the Ansoft HFSS modeling tools to analyze coupling between the antenna feed port and optical ports assigned on the split directors of the quasi-Yagi antenna (Fig. 9). The optical ports provide electrical connection between the external edges of the pads (antenna directors) and nearby bottom

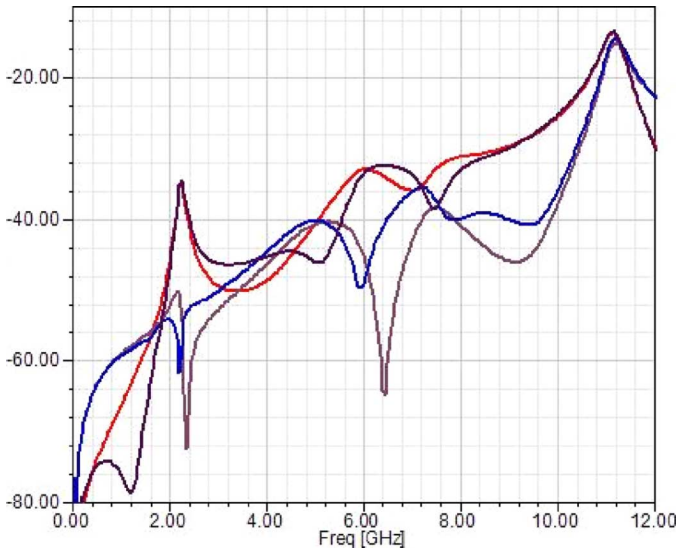

Fig. 10. Ansoft HFSS predicted coupling in decibels between the antenna port and four optical ports which are formed for the split antenna directors used also as the optical component pads. Different plot colors are used for different port combinations for all four optical ports.

(system) ground. Bonding wires are also added to the computer model to support electrical connection required for optical active components placed on the pads. Collectively, such ports and wires form the closed ac and dc signal paths. This level of details is sufficient to predict the EM coupling effects.

In this model, the simulated return loss is very similar to that in Fig. 4 computed with the CST Microwave Studio software and is not shown here. Electromagnetic coupling appears between the RF and optical ports in the structure shown as in Fig. 9 because of the shared onboard structural elements used simultaneously as the antenna directors and optical circuit pads. The computed magnitude of EM coupling, which is observed between the antenna port and four optical ports, is plotted in Fig. 10 with respect to the 50 Ω reference impedance. Specifically, the coupling approaches the magnitude of 15–20 dB in the antenna operational band around 10 GHz for the simulated layouts pictured in Fig. 9. This estimated coupling level might appear as negligible in the case of optical transmitters but it might exhibit a perceptible effect in the optical receiver as studied in Section V. In particular, the estimated coupling in Fig. 10 allows evaluation of signal distortions in dual mode RF-optical links when a week optical received signal is parasitically coupled to a much stronger RF transmit signal and vise versa.

V. Measurement of FSO Link

A. Optical Transmitter on Antenna Board

To investigate experimentally the electromagnetic coupling between the RF and optical circuits, the optical transmitter is tested first. The setup for transmitter measurement is shown schematically in Fig. 11. A pulse pattern generator (PPG, Anritsu MP1800A) is connected to the RF/opto transmitter board by SMA cables. A 2.5 Gb/s $2^7 - 1$ PRBS signal is fed into the laser driver circuit to modulate the VCSEL. VCSEL optical emission is collimated by a lens with 5 mm focal length. Through an objective lens, the beam is then coupled into a multimode fiber on a precision fiber launch system. A high-speed commercial receiver (F425S17485 Small Form Factor Pluggable transceiver module) is connected to the multimode fiber to detect the received optical signal. The differential receiver output signal is viewed on a digital sampling oscilloscope (Agilent DCA-J 86100C).

The antenna EM time-varying fields induce unavoidably certain current in the optical circuits because of the sharing of structural components as revealed in Section IV. Furthermore, the simulation from CST microwave studio shows that the amplitude of the induced current is $\sim 2.5\ \mu$A when the antenna fed power is 30 dBm. For the optical transmitter in our system, the VCSEL modulation current is set to 6 mA by the laser driver circuit. Typically, the antenna fed in power is much less than 30 dBm for a line-of-sight (LOS) operation. Therefore, the simulation results suggest that the antenna radiation will not affect the transmitter performance even though the VCSEL is placed in the near field of the antenna and the sharing of the antenna director pads. To verify the simulation, we test the eye diagram of the FSO link when the antenna is turned off, and turned on with a feed power of 14 dBm for CW signals. As shown in Fig. 12, no noticeable change in eye diagram is observed between the two scenarios, thus validating the simulation results.

However, parasitic inductances and capacitances associated with electrical leads, packaging, and laser diode cause degradation in the high frequency characteristics of the optical transmitter waveform. Such parasitics imposes constraints on the maximum achievable data transmission rate. To evaluate the observed ringing behavior in the laser driver output waveform, a simplified second-order response output circuit is shown in Fig. 13. The capacitance $\mathrm{C_{out}}$ includes the capacitance associated with the laser driver circuit output pin, $\mathrm{L_{bond}}$ is the bond wire inductance connecting the Duroid board to the PCB, and the laser diode is approximated by a parallel $\mathrm{R_D}$, $\mathrm{C_D}$ equivalent circuit. The simulation by Ansoft Maxwell 2-D reveals that the capacitance between two antenna director pads is about 18.61 pF and the capacitance between bonding wires is about 7.67 pF. These two component value are included in $\mathrm{C_D}$. The capacitance of bonding pads on PCB is 9.18 pF, which is included in $\mathrm{C_{out}}$. As the LD modulation current switches, a slowly decaying ringing response is present in the drive current waveform. The resonance frequency of the series LC circuit in Fig. 13 is given by

$$f_o = \frac{1}{2\pi\sqrt{\frac{L_{\mathrm{bond}}C_{\mathrm{out}}C_{\mathrm{D}}}{C_{\mathrm{out}}+C_{\mathrm{D}}}}}. \tag{2}$$

Based on reported component values from device datasheets and simulations, the resonance frequency is approximately 1.75 GHz and decreases as the bond wire inductance increases. The measured transient output waveform of optical transmitter at 1 Gb/s is shown in Fig. 14. The ringing effect appears as predicted by theoretical calculation. To minimize the signal

Fig. 11. Block diagram of optical transmitter test setup.

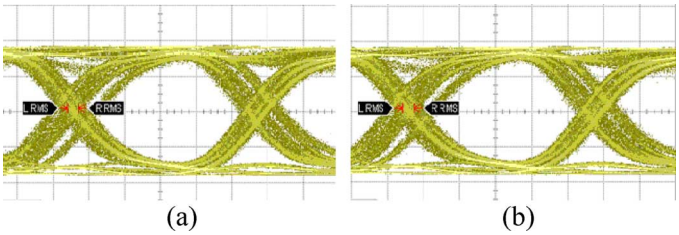

Fig. 12. Measured eye diagram at 2.5 Gb/s when antenna is (a) turned off and (b) fed with 14 dBm CW signal.

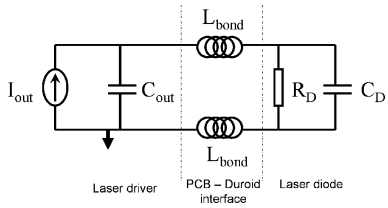

Fig. 13. Simplified equivalent circuit for output waveform analysis.

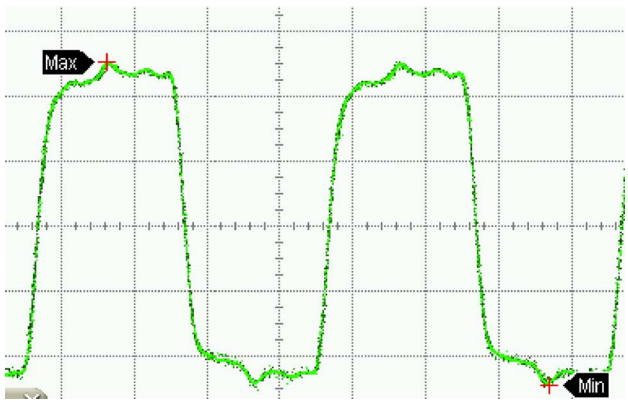

Fig. 14. Transient waveform of optical transmitter at 1 Gb/s.

distortion, capacitive structure such as metal pads and long bonding wire pairs need to be revised in future design.

B. Optical Receiver on Antenna Board

For the optical receiver testing, the setup is shown in Fig. 15. A commercial optical transmitter (F425S17485 Small Form Factor Pluggable transceiver module) is used to generate the optical transmitter signal, which is driven by a 2.5 Gb/s $2^7 - 1$ PRBS signal from the PPG. The laser beam is coupled into a multimode fiber and routed to the PIN photodiode through a fiber probe. The RF/opto receiver board detects the optical signal and converts it into a differential voltage signal that is finally displayed on the oscilloscope.

As the antenna induced current flows along the same path as the photocurrent does, the noise current will be amplified by the TIA. From the datasheet, we know that the transimpedance of TIA is 2.75 kΩ in linear region and the responsivity of the PIN is 0.6 A/W. If all the power from VCSEL (1.5 mW) is collected by the PIN diode as for ideal case, the photocurrent at the PD is 0.9 mA. In this case, the noise current is much smaller than the photocurrent. However, when the optical link is not perfectly aligned, the collected power is smaller than the ideal case; therefore the noise can be comparable to the signal. For example, if the noise current is 2.5 μA at TIA input, the noise voltage at TIA output will be 6.875 mV. This noise is not negligible when the light collected by PIN diode is small. To experimentally demonstrate the effect of antenna induced current noise, we tested the receiver board when the optical power collected by PIN is $\sim 50\,\mu$W. From the transient output waveform shown in Fig. 16(d), it is observed that noise voltage is comparable to signal.

We use a simple link model [Fig. 17(a)] programmed by Matlab to quantify the mutual coupling phenomenology in the case of receivers. The Matlab model composes of several computational modules. First, two signal sources are calculated including PRBS [Fig. 17(b)] and a random-phase continues wave (CW) signal. Then, both signals are summed with a weight (W) that depends on the level of inter-channel coupling. Finally, the eye diagram of the resulted signal is computed. The Matlab model employs the level of electromagnetic coupling computed through full wave EM simulations in Section IV. We utilize the $2^7 - 1$ PRBS optical signal transmitted at 2.5 Gb/s rate which is the same as used for measurements with the optical transmit and receiver boards. Further, a RF time harmonic signal at 10 GHz is added to the PRBS test sequence as a noisy signal component. The magnitude of the additive noise signal corresponds to the predicted value of the inter-channel coupling that is the weight W in Fig. 17(a) accordingly to the Fig. 10, while its phase is set to random because the optical and RF signals are presumably phase unlocked. A portion of the transmitted $2^7 - 1$ PRBS under such channel conditions is plotted in Fig. 17(b). The eye diagram for the channel signal as in Fig. 17(b) is depicted in Fig. 17(c) and indicates degradation of the received signal.

The simulated data eye diagram [Fig. 17(c)] is in good agreement with measured results for the same signal and bit rate in the RF/opto receiver (Fig. 18). Besides, it is important to note that the results in Fig. 16(d) and Fig. 18(d) are demonstrated for the worst case regarding EM coupling to optical receiver. For general applications, the antenna on the receiver board operates in receiving mode and the RF power absorbed by the antenna is much lower than 14 dBm; therefore the EM induced noise should be minimal.

Degradation in the received signal waveform is also observed due to the parasitic inductance and capacitances associated with the equivalent circuit at the Duroid-PCB interface, connecting the photodetector to the front-end TIA circuit. A similar circuit

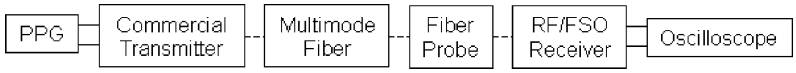

Fig. 15. Block diagram of optical receiver test setup.

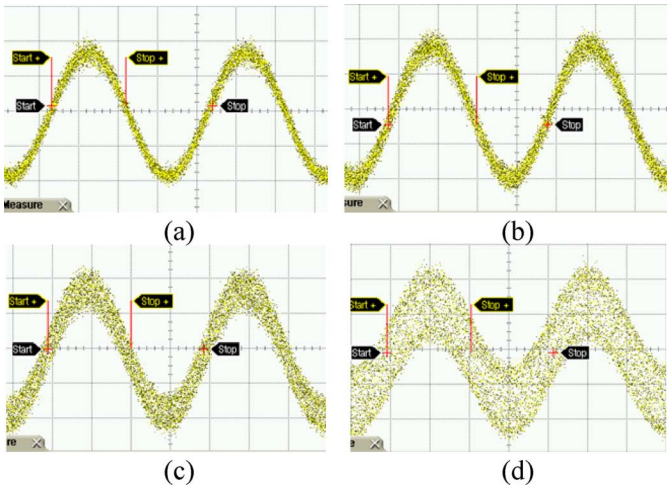

Fig. 16. Transient output waveform when antenna is (a) turned off and fed by (b) 0 dBm, (c) 7 dBm, (d) 14 dBm CW signal.

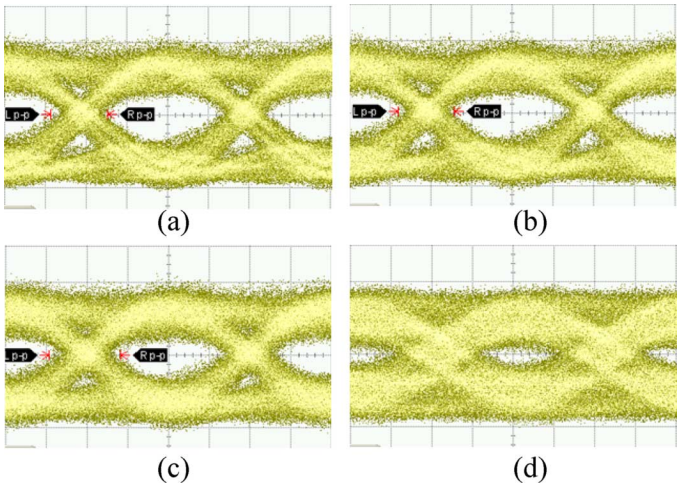

Fig. 18. Measured eye diagram for optical receiver at 2.5 Gb/s $2^7 - 1$ PRBS when antenna is (a) turned off or fed by (b) 0 dBm, (c) 7 dBm, (d) 14 dBm CW signal.

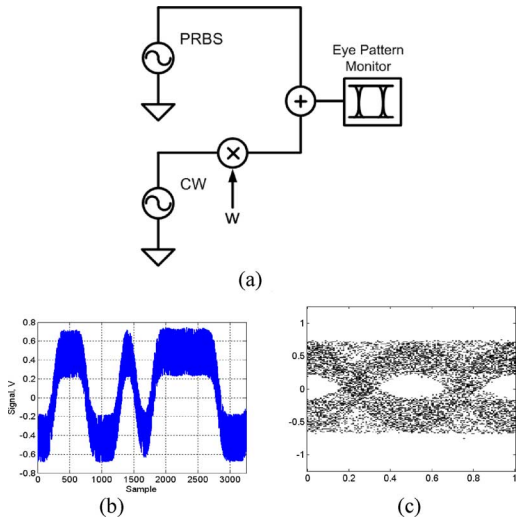

Fig. 17. (a) Schematic structure of Matlab lab for eye diagram modeling. (b) A portion of the test $2^7 - 1$ PRBS mixed with random phase time-harmonic signals at the frequency around 10 GHz. (c) Computed eye diagram for (b).

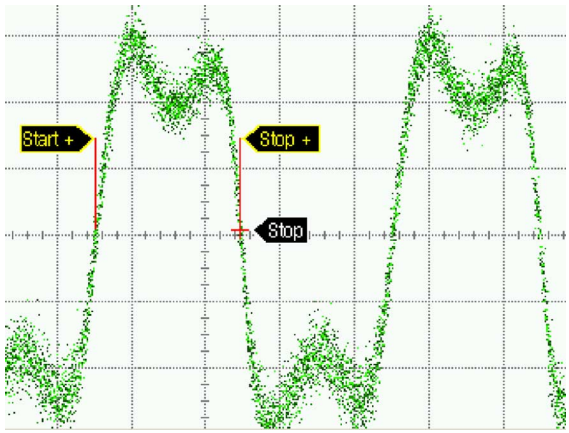

Fig. 19. Ringing of receiver at 1 Gb/s.

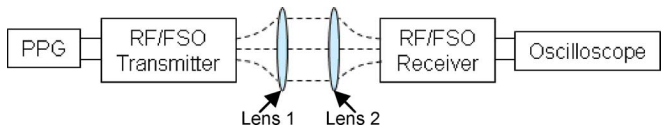

Fig. 20. Block diagram of FSO link test setup.

to Fig. 13 is used to analyze the high-frequency behavior of the optical receiver output. The observed ringing in the transient response is at 1.2 GHz (Fig. 19).

C. FSO Link at 2.5 Gb/s

To demonstrate the feasibility of FSO communication under antenna near field radiation, a RF/FSO dual mode transmitter-receiver link is implemented. The transmitter and receiver are both mounted on XYZ translation stages for the purpose of beam alignment. Two lenses with 25 mm focal length are used to collimate and focus the laser beam. The separation between the transmitter and the receiver board is 25 cm. For beam alignment, we first adjust the position of Lens 1 placed in front of the RF/FSO transmitter until the output beam is collimated. Next, we adjust Lens 2 in front of the RF/FSO receiver to focus the optical beam on the PIN. Finally, the position of the PIN is tuned for maximum photocurrent signal. The block diagram of the test setup is shown in Fig. 20.

In this setup, the RF signal is fed into the antenna on the transmitter board while the antenna on the receiver board is connected to a spectrum analyzer to measure the received RF power. When the transmitting antenna is fed with 14 dBm CW signal at 10 GHz, the received RF power is -14 dBm. As previously

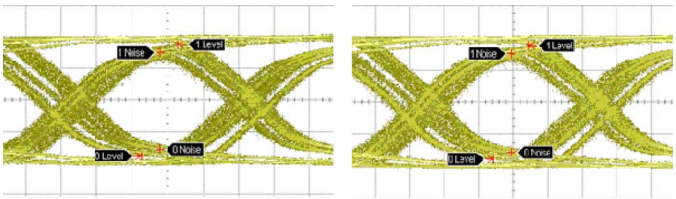

Fig. 21. Measured eye diagram for FSO link at 2.5 Gb/s $2^7 - 1$ PRBS when antenna on transmitter board is (a) turned off and (b) fed by 14 dBm signal.

discussed, the antenna near field radiation has little effect on the transmitter side and can be neglected on the receiver side if the RF receiving power is small. Therefore, the coupling from RF channel to FSO channel is negligible in this setup. The measured eye diagrams when the antenna is turned off or on are shown in Fig. 21. No noticeable change in the eye diagram is observed when the antenna is on or off, validating the theoretical prediction.

VI. Conclusion

An ultra compact RF/opto transceiver modular design is developed for RF/FSO dual mode wireless communication represented by optical transmitter and receiver boards integrated with PCB antenna. In this modular design, optical transceiver front-end (VCSEL/PIN) is packaged with RF front-end antenna with shared structural components. The split director of the modified Yagi antenna serves as an electrical contact for the VCSEL and PIN devices and as resonant structures for EM radiation through the RF channel. Measurement of the antenna radiation pattern reveals that the RF channel performance is not degraded by the optical signal. Simulation and experimental results suggest that the antenna near field radiation has negligible effect on the optical channel performance. FSO link transmission at 2.5 Gb/s in a 10 GHz RF environment is achieved. However, the coupling from the RF signal to electrical interconnections at the optical receiver is not negligible when the received optical power is low. The parasitic inductance and capacitances introduced by electrical connections at the interface between the VCSEL/PIN devices and packaged laser driver/TIA circuits introduce ringing in the transient signal. The future study of this topic will focus on a fully integrated RF/opto transceiver using bare die laser driver/TIA circuits flip-chip bonded to the optoelectronic devices to minimize packaging and electrical interconnection parasitics. In addition, compact antenna structures, including microstrip patch antennas, will be investigated for dual-mode transceiver integration.

References

[1] T. Kamalakis, I. Neokosmidis, A. Tsipouras, T. Sphicopoulos, S. Pantazis, and I. Andrikopoulos, "Hybrid free space optical/millimeter wave outdoor links for broadband wireless access networks," in *18th Annu. IEEE Int. Symp. Personal, Indoor Mobile Radio Commun. (PIMRC'07)*, Sep. 2007, pp. 1–5.

[2] T. Rokkas, T. Kamalakis, D. Katsianis, D. Varoutas, and T. Sphicopoulos, "Business prospects of wide-scale deployment of free space optical technology as a last-mile solution: A techno-economic evaluation," *J. Optical Networking*, vol. 6, no. 7, pp. 860–870, Jul. 2007.

[3] The last-mile solution: Hybrid FSO radio, white paper Airfiber, 2002.

[4] E. Leitgeb, M. Gebhart, U. Birnbacher, W. Kogler, and P. Schrotter, "High availability of hybrid wireless network," in *Proc. SPIE*, Strasbourg, Apr. 2004, vol. 5465, pp. 238–249.

[5] H. Izadpanah, T. ElBatt, V. Kukshya, F. Dolezal, and B. K. Ryu, "High-availability free space optical and RF hybrid wireless networks," *IEEE Wireless Commun.*, vol. 10, no. 2, pp. 45–53, Apr. 2003.

[6] S. D. Milner and C. C. Davis, "Hybrid free space optical/RF networks for tactical operations," in *IEEE Military Commun. Conf.*, Oct.–Nov. 2004, vol. 1, pp. 409–415.

[7] B. W. Cook, S. Lanzisera, and K. S. J. Pister, "SoC issues for RF smart dust," *Proc. IEEE*, vol. 94, no. 6, pp. 1177–1196, Jun. 2006.

[8] J. J. Lin, L. Gao, A. Sugavanam, X. Guo, R. Li, J. E. Brewerand, and K. K. O, "Integrated antennas on silicon substrates for communication over free space," *IEEE Electron Device Lett.*, vol. 25, no. 4, pp. 196–198, Apr. 2004.

[9] F. Touati and M. Pons, "On-chip integration of dipole antenna and VCO using standard BiCMOS technology for 10 GHz applications," in *Proc. 29th Eur. Solid-State Circuits Conf.*, Sep. 2003, pp. 493–496.

[10] Y. Su, J. J. Lin, and K. K. O, "A 20 GHz CMOS RF down-converter with an on-chip antenna," in *IEEE Proc. ISSCC*, Feb. 2005, vol. 1, pp. 270–597.

[11] H. Hashemi1, X. Guan, and A. Hajimiri, "A fully integrated 24 GHz 8-path phased-array receiver in silicon," in *IEEE Int. Solid-State Circuits Conf.*, Feb. 2004, vol. 1, pp. 390–534.

[12] O. E. Erdogan, R. Gupta, D. G. Yee, J. C. Rudell, J. Ko, R. Brockenbrough, S. Lee, E. Lei, J. L. Tham, H. Wu, C. Conroy, and B. Kim, "A single-chip quad-band GSM/GPRS transceiver in 0.18 μm standard CMOS," in *IEEE Int. Solid-State Circuits Conf.*, Feb. 2005, vol. 1, pp. 318–601.

[13] K. K. O, K. Kim, B. A. Floyd, J. L. Mehta, H. Yoon, C. Hung, D. Bravo, T. O. Dickson, X. Guo, R. Li, N. Trichy, J. Caserta, W. R. Bomstad, II, J. Branch, D. Yang, J. Bohorquez, E. Seok, L. Gao, A. Sugavanam, J. J. Lin, J. Chen, and J. E. Brewer, "On-chip antennas in silicon ICs and their application," *IEEE Trans. Electron Devices*, vol. 52, no. 7, pp. 1312–1323, Jul. 2005.

[14] W. R. Deal, N. Kaneda, J. Sor, Y. Qian, and T. Itoh, "A new quasi-Yagi antenna for planar active antenna arrays," *IEEE Trans. Microwave Theory Tech.*, vol. 48, no. 6, pp. 910–918, Jun. 2000.

[15] J. Liao, S. Deng, K. A. Connor, V. Joyner, and Z. R. Huang, "Antenna integration with laser diodes and photodetectors for a miniaturized dual-mode wireless transceiver," in *Proc 58th IEEE Electron. Compon. Technol. Conf.*, May 2008, pp. 1864–1868.

[16] F. W. Grover, *Inductance Calculations: Working Formulas and Tables*. Mineola, NY: Dover.

[17] C. A. Balanis, *Antenna Theory: Analysis and Design*, 2nd ed. New York: Wiley, 1997, pp. 622–625.

[18] S. Gregson, J. McCormick, and C. Parini, *Principles of Planar Near-Field Antenna Measurements*. London, U.K.: IET, 2007.

[19] S. E. Melais and T. M. Weller, "A quasi Yagi antenna backed by a metal reflector," *IEEE Trans. Antennas Propagat.*, vol. 56, no. 12, pp. 3868–3872, Dec. 2008.

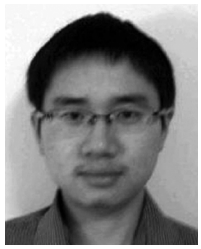

Jun Liao (M'07) received the B.S. degree from Beijing University of Posts and Telecommunications, Beijing, China, in 2006. He is currently pursuing Ph.D. degree in the Department of Electrical, Computer and Systems Engineering, Rensselaer Polytechnic Institute, Troy, NY.

His research interest includes RF/opto hybrid packing, planar antenna design, and free space optical communication.

Juan Zeng (M'03) received B.S. degree in electronic science and technology from the Harbin Institute of Technology (HIT), Harbin, China, in 2007. She is currently working toward the M.S. degree in electrical engineering at Tufts University, Medford, MA.

Her research interests include CMOS circuits for broadband wireless applications.

Ms. Zeng received MediaTek Inc. & Wu Ta-You Scholar Award from Harbin Institute of Technology in 2006 and the Dean's Fellowship from Tufts University in 2007.

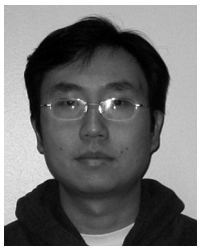

Shengling Deng (M'08) received the B.S. in physics at Nanjing University, China, in 2002, and the M.S. in electrical engineering at University of Florida, in 2005. He is currently working toward the Ph.D. degree at Rensselaer Polytechnic Institute, Troy, NY.

His research interest includes III-V MSM integration, Si-based EO modulator, and integrated optics on SOI.

Anatoliy O. Boryssenko received the M.Sc. E.E. and Ph.D. E.E. degrees from the Kiev Polytechnic Institute, Kiev, Ukraine.

He worked as an Associate Professor of the Kiev Polytechnic Institute and as a Research and Development Engineer in companies related to millimeter-wave and UWB communication and sensor systems. Research interests include subsurface radar imaging, broadband and UWB antenna and array design, applied and computational electromagnetics, signal processing and system design for radar, sensing and imaging. Since 2000, he works the University of Massachusetts, Amherst. Now he is a Research Associate Professor of the ECE Department.

Valencia M. Joyner (M'98) received the S.B. and M.Eng. degrees in electrical engineering and computer science from the Massachusetts Institute of Technology, Cambridge, in 1998 and 1999, respectively, and the Ph.D. degree from the University of Cambridge, Cambridge, U.K., in 2003.

She is currently an Assistant Professor at Tufts University, Medford, MA, where she leads the Advanced Integrated Circuits and Systems Group. Her current research interests include opto-electronic integrated circuit design for high-speed optical and RF wireless networks and biomedical imaging applications.

Dr. Joyner was awarded a Marshall Scholarship and NSF Graduate Research Fellowship.

Zhaoran Rena Huang (M'99) received the B.S. degree from the Beijing Institute of Technology, Beijing, China, in 1995, the M.Sc. and Ph.D. degrees from the Georgia Institute of Technology, Atlanta, in 1999 and 2003, respectively.

She is currently an Assistant Professor at Rensselaer Polytechnic Institute, Troy, NY. Her current research focus includes RF/opto packaging for high-speed low power wireless communication, and integrated silicon photonics for next-generation lightwave technology.